

SUPPLEMENTARY INFORMATION

Polymer-based Microfluidic Device for On-chip Counter-diffusive Crystallization and *In Situ* X-ray Crystallography at Room Temperature

Sarthak Saha,¹ Can Özden,² Alfred Samkutty,² Silvia Russi,³ Aina Cohen,³ Margaret M. Stratton,² Sarah L. Perry¹

¹Department of Chemical Engineering, University of Massachusetts Amherst, MA 01003, USA

²Department of Biochemistry and Molecular Biology, University of Massachusetts Amherst, MA 01003, USA

³SLAC National Accelerator Laboratory, Menlo Park, CA 94025, USA

S1. Device Fabrication and Characterization

Photolithography allows for the direct creation of features without the need for etching. We used spin coating to define the layer thickness of the SU-8 photoresist used to create the device according to the datasheet provided by the manufacturer (Kayaku Advanced Materials). The open-faced channel layer was fabricated using SU-8 2100 at 2000 rpm to achieve a thickness of 113 μm . This was thermally sealed with a layer of SU-8 2010 using nanoimprinter (Nanonex, Monmouth Junction, NJ, USA) at 10 psi (68.95 kPa) and 69°C (Figures S1a,b). When viewed under a microscope, we observed that the thermal bonding at high pressure, caused the SU-8 film to sag in the large crystallization chamber. We validated our observation using optical profilometry (Zygo Nexview) and a dip of 30 μm was observed (Figure S1d). Hence the resulted thickness of the reaction chamber ranged from 83 μm at the center to 113 μm at the edges.

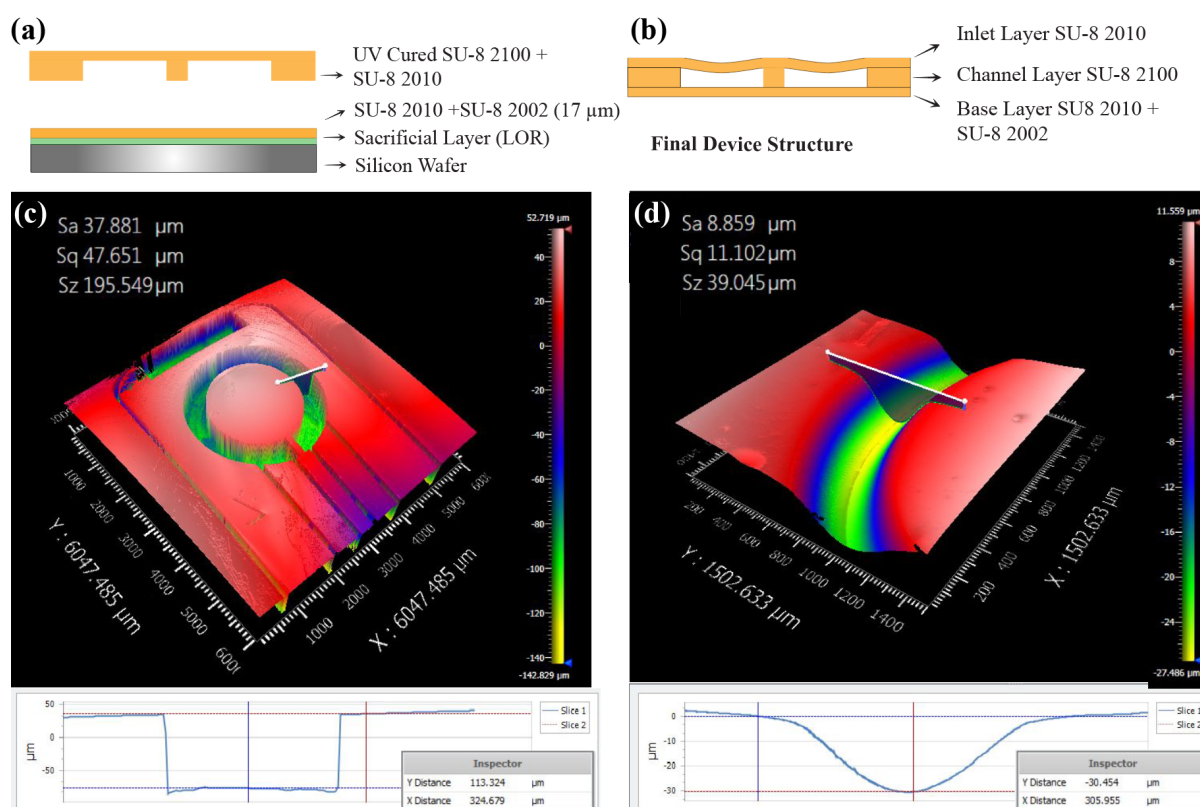


Figure S1. (a) Schematic of the device architecture used during nanoimprint lithography used to bind two layers of SU-8, and (b) the corresponding distortion in the polymer film observed from the process. Profilometry images (c) depicting the 113 μm thickness of the open faced channel layer before being bonded to the base layer and (d) the 30 μm dip observed in the bonded structure on the top of the channel layer after the nanoimprinting.

In order to bolster the centrifugal valve, a hydrophobic tridecafluoro-1,1,2,2-tetrahydrooctyl)trichlorosilane (Gelest Inc., Morrisville, PA, USA) was selectively deposited using vapour treatment under vacuum (Figure S2f). As shown in Figure S2e, the device was covered with a silicone sheet so as to mask the inlet holes and metering vents while allowing the valve opening being accessible to the silane vapour. The treatment yielded a change in static contact angle from 53° to 99° (Figures S2b,c). The contact angle measurement also indicated that freshly crosslinked SU-8 is close to being hydrophobic at 84°. However, we

observed that the overnight exposure to the RD6 developer needed to remove the sacrificial LOR3A also served to increase the hydrophilicity of SU-8. We observed that the contact angle of native SU-8 changed from 84° to 53° after RD6 treatment (Figures S2a,b).

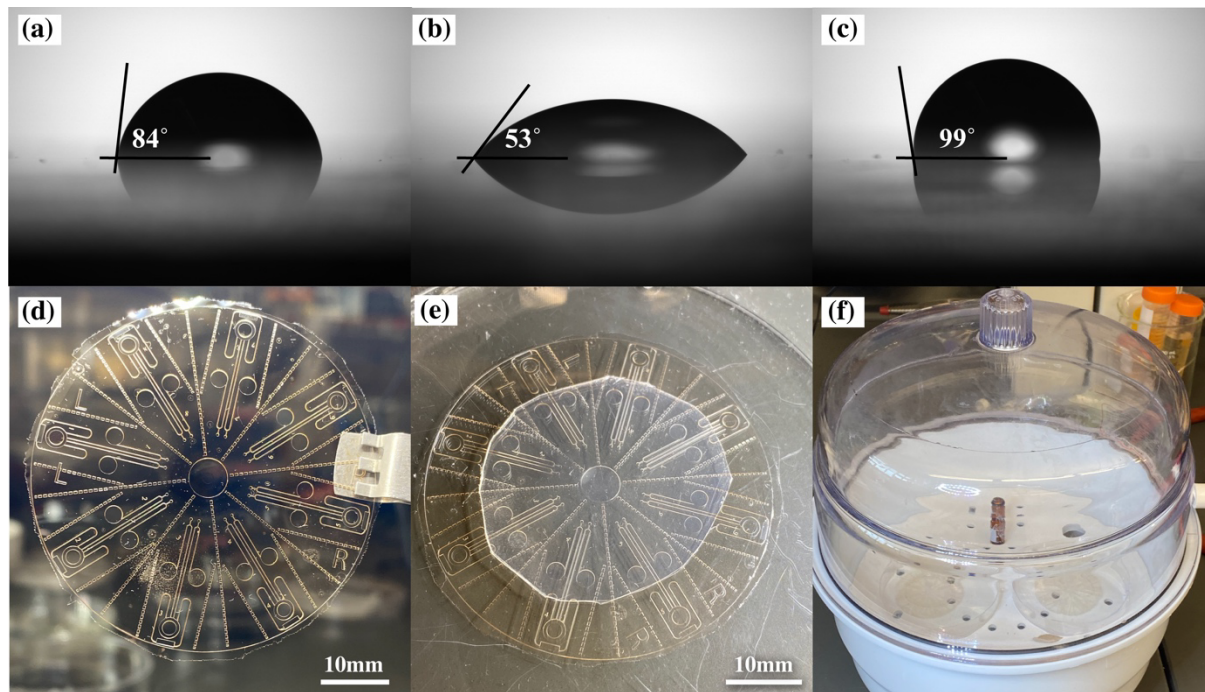


Figure S2. Contact angle of water on (a) freshly crosslinked SU-8 (b) after overnight RD6 treatment and (c) after silane treatment. Photographs of (d) the overall device, (e) a device covered with silicon sheet exposing the valves for silane deposition, and (f) silane deposition occurring on the covered devices in a vacuum chamber.

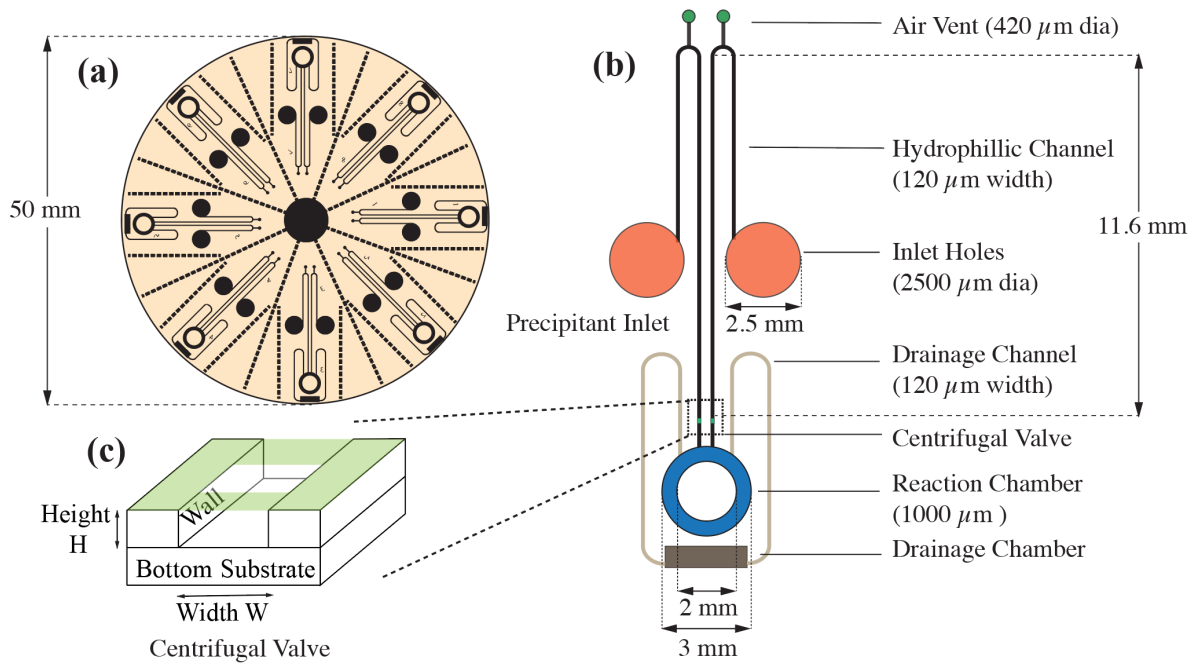


Figure S3. Schematic of the (a) overall device design, (b) a zoomed in schematic of each individual section showing the dimensions of all the features, and (c) a 3D schematic of the centrifugal valve.

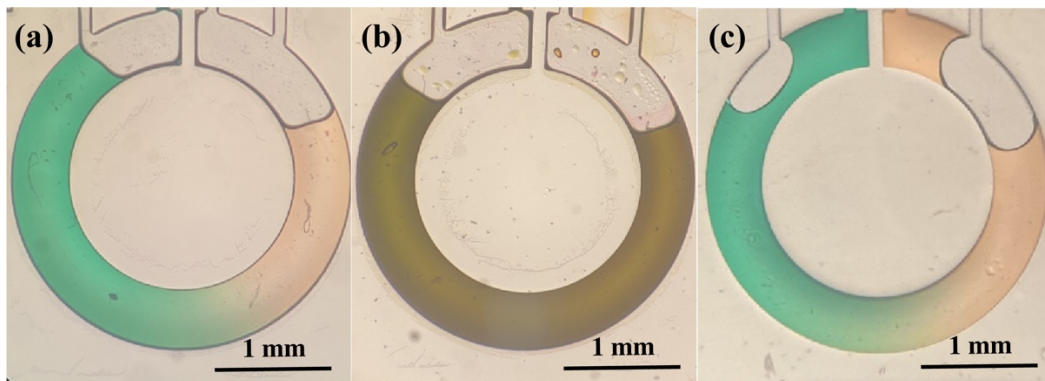


Figure S4. Optical micrographs of a device containing food dye when (a) mixed at 1500 rpm using a spin coater, (b) mixed at 2500 rpm using a spin coater, and (c) mixed via multiple flicks of the hand and no other ancillaries.

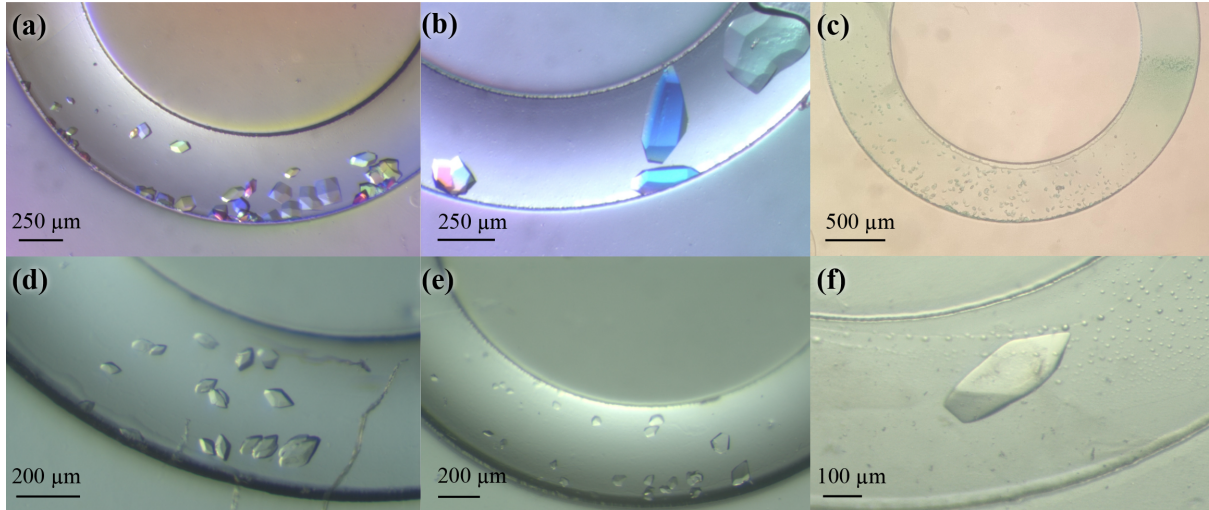


Figure S5. (a)-(c) Polarized optical micrographs showing protein crystals of lysozyme grown on-chip. (d)-(f) Optical micrographs of the hub domain of human CaMKII β grown on-chip.

S2. X-ray Compatibility

When selecting materials for X-ray compatible microfluidic devices, it is important to consider the transparency of the material, or the degree to which the incident X-rays become attenuated upon transmission through the material. Attenuation is caused by the absorption of photons, resulting in decreased intensity of both the incident X-ray beam and the resulting signal. The attenuation of X-rays can be calculated for any given X-ray energy based on the exponential decay of the incident intensity I_0 of monochromatic photons as they travel through a material of thickness x and a linear attenuation coefficient μ .¹⁻³

$$I = I_0 \exp(-\mu x) \quad (\text{S1})$$

Attenuation coefficients⁴⁻¹⁰ have been well documented in the literature for elemental materials, as the attenuation is directly a function of the electron density of the material.² Starting from a mass attenuation coefficient (μ/ρ), which has been determined experimentally based on measurements of intensity vs. thickness, we calculate the corresponding linear attenuation coefficient of each element (μ). For a compound containing multiple elements, the linear attenuation coefficient can be calculated as a weighted average of the individual elements i based on their mass fraction w_i .

$$\mu = \sum \mu_i w_i \quad (\text{S2})$$

Table S1 lists the chemical composition and the respective atomic mass fraction of the various materials used commonly for the fabrication of microfluidic devices. These include polydimethylsiloxane (PDMS), which is widely used in various microfluidic devices, silicon nitride, and polyimide (Kapton) which have often been reported as X-ray compatible materials, and SU-8, as used here. From the attenuation coefficient, we calculated the transmission factor I/I_0 at a photon energy of 12.4 keV, or a wavelength of 1Å, as shown in Figure S6.

Attenuation coefficients are a function of atomic number and density, which explains the low attenuation and hence high transmission factor for air. Furthermore, for the same material thickness, organic polymers like SU-8 and polyimide have higher transmission as compared to silicon containing materials because of the differences in atomic number and density.

In the context of the devices reported here, we have found that it is necessary to maintain a device material thickness of 10-20 μm to have the required strength to support physical handling and device operation. In this range of thicknesses, Figure S6 shows that polymeric materials provide a high transmission factor of 97-98%.

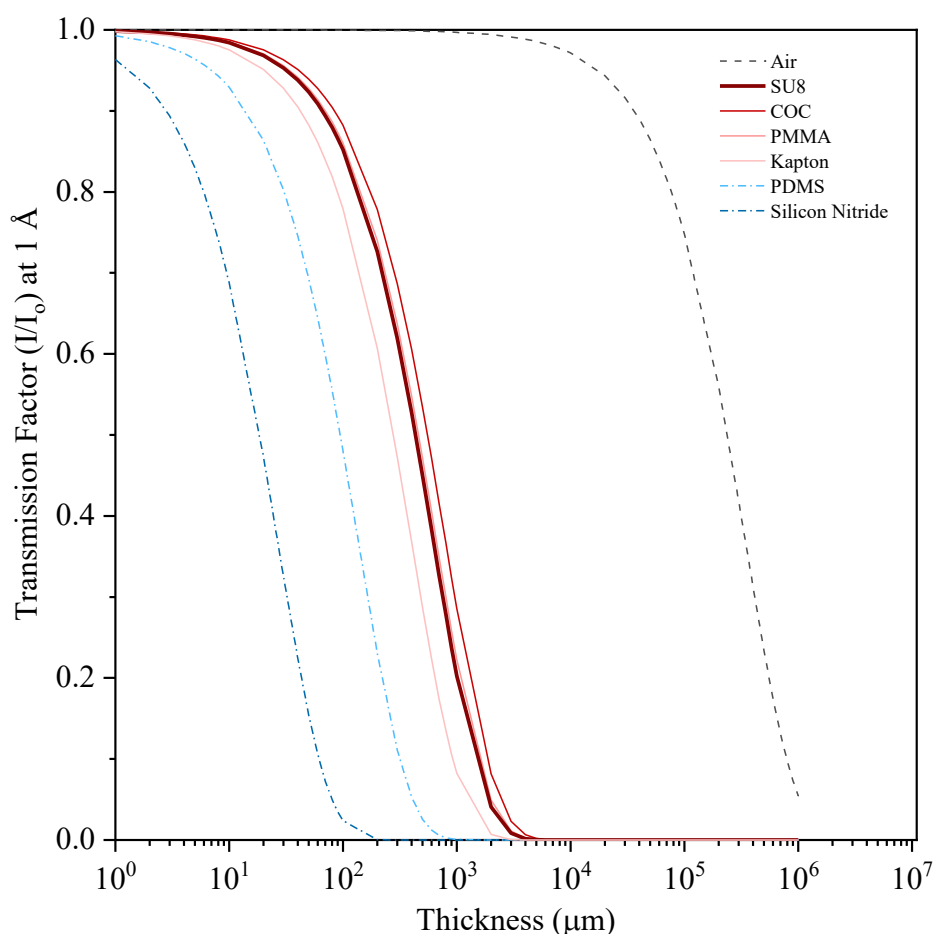


Figure S6. A comparison of the transmission factors I/I_0 vs. thickness for varying materials at an X-ray energy of 12.4 keV, or a wavelength of 1Å.

Table S1. Atomic mass fraction, density, and the corresponding calculated value of the linear attenuation coefficient μ at 1Å (12.4 keV) for different materials typically used in the fabrication of microfluidic devices.

	Air	PDMS	Silicon Nitride	COC	PMMA	SU-8	Kapton
Elements		$\text{Si}_{61}\text{O}_{60}\text{C}_{124}\text{H}_{368}$	Si_3N_4	C_9H_4	$\text{C}_5\text{H}_8\text{O}$	$\text{C}_{91}\text{O}_{16}\text{H}_{86}$	$\text{C}_{22}\text{H}_{10}\text{N}_2\text{O}_5$
Mass Fraction	H	0.08182		0.11546	0.09586	0.06	0.02636
	C	0.0015	0.32853	0.88454	0.71394	0.76	0.69118
	N	0.75518		0.39938	0.00000		0.07328
	O	0.23179	0.21175		0.19020	0.18	0.20918
	Si		0.37791	0.60062			0.00000
	Ar	0.01288					
Density (g/cm³)	0.001225	0.92	3.2	1.02	0.94	1.218	1.42
μ (cm⁻¹) at 1Å	0.00290562	7.3343673	37.41605	1.253462	1.503741	1.59746	2.496832

S3. X-ray Crystallography and Crystal Isomorphism

We analyzed the statistical variation of the unit cell parameters for the CaMKII β hub domain crystals. After indexing and geometrical refinement of each crystal, the analysis was performed using methods described by Q. Liu *et al.*^{11,12} A standard Euclidean distance, $\Delta_{j,k}$ was used to calculate the variation in crystal unit cell parameter. The Euclidean distance is a normalized distance using the unit cell parameter a , b , c , α , β , and γ of crystal j and k across N different crystals. It is normalized using the variance of these parameters over the population.

$$\Delta_{j,k} = \left[\frac{1}{\sigma^2} \sum_{u=a,b,c,\alpha,\beta,\gamma} (u_j - u_k)^2 \right]^{\frac{1}{2}} \quad (\text{S3})$$

$$\sigma^2 = \left[\frac{1}{N} \sum_{k=1}^N (u_k - \bar{u}_k)^2 \right] \quad (\text{S4})$$

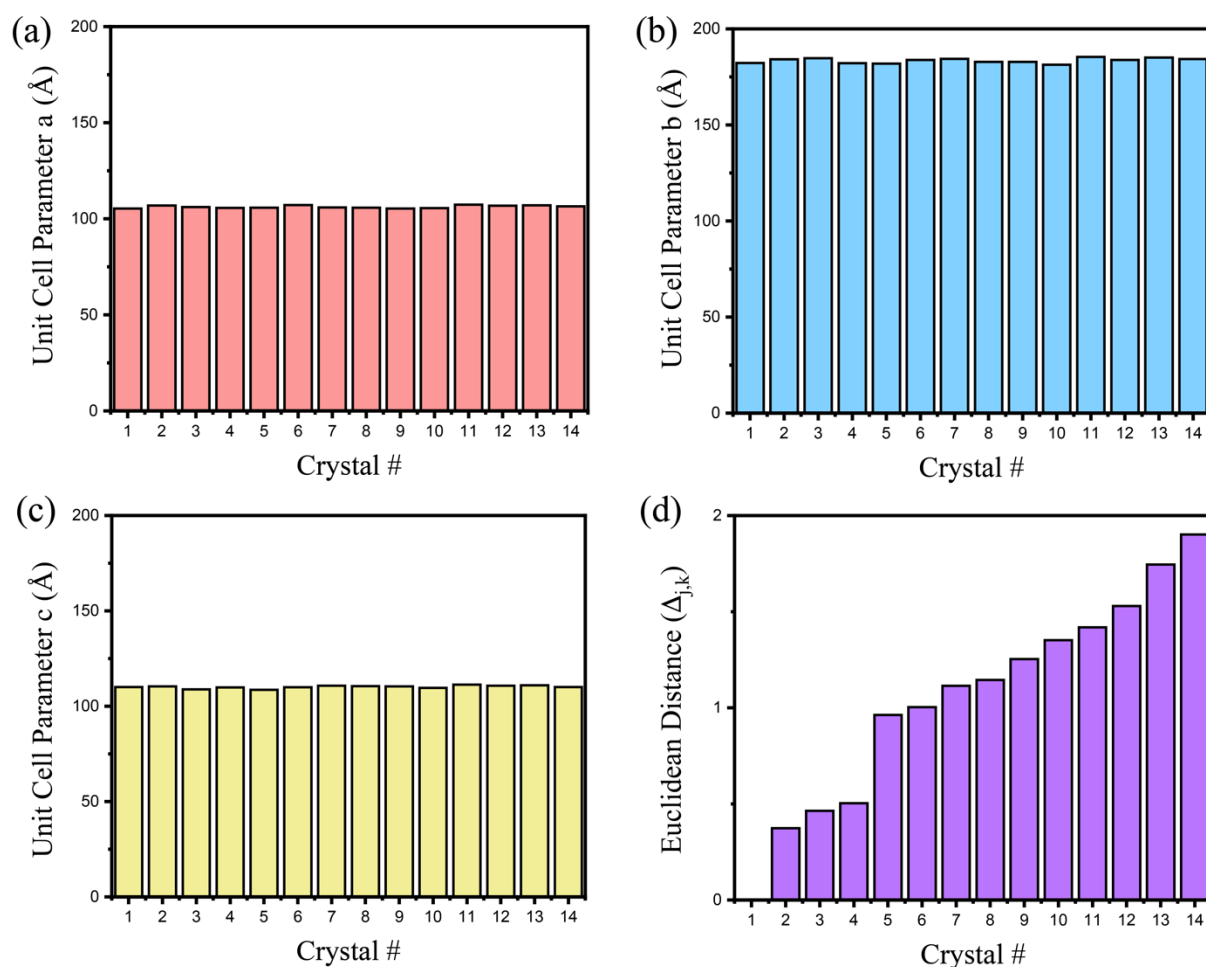


Figure S7. (a)-(c) Plot of the variation in the corresponding unit cell parameter across the 14 crystals of CaMKII β analyzed, and (d) a plot of the standard Euclidean distance $\Delta_{j,k}$ vs. crystal, showing the variation in the unit cell parameters.

Table S2. Crystallographic statistics for data obtained using on-chip and cryogenic analysis of CaMKII β .

	CaMKII β hub domain (PDB:7URW) (crystals grown in well plate and data collected in cryogenic condition)	CaMKII β hub domain (PDB:7URY) (crystals grown and data collected on chip at room temperature)
Data collection		
Space group	C222 ₁	C222 ₁
Cell dimensions		
a, b, c (Å)	104.24, 183.19, 108.37	105.71, 182.8, 110.52
α, β, γ (°)	90, 90, 90	90, 90, 90
Resolution (Å)	50 – 3.10 (3.15 – 3.10)	50 – 2.64 (2.69 – 2.64)
R_{merge}	0.291 (1.454)	0.072 (0.443)
Mean $I/\sigma I$	6.2 (1.67)	4.4 (1.86)
Completeness (%)	98.5 (95.4)	88.9 (91.5)
Redundancy	6.2 (5.5)	3.6 (3.7)
CC _{1/2}	0.962 (0.567)	0.997 (0.826)
CC*	0.990 (0.851)	0.999 (0.951)
Refinement		
Resolution (Å)	37.8 – 3.11 (3.186 – 3.11)	38.23 – 2.64 (2.707 – 2.64)
Unique reflections	17703 (1200)	26822 (1942)
$R_{\text{work}} / R_{\text{free}}$ (%)	25.7/30.02	20.37/23.53
No. atoms		
Protein	6789	7036
Water	-	-
Ligand	-	36
Ramachadran plot		
In preferred regions (%)	97.54	98.86
In allowed regions (%)	1.75	1.02
Outliers (%)	0.70	0.11
B -factors		
Protein	74.74	58.1
Water	-	-
Ligand	-	85.71
R.M.S. deviations		
Bond lengths (Å)	0.0046	0.0044
Bond angles (°)	1.3269	1.3236

^a Statistics for the high-resolution shell are indicated between brackets

^b Comparison of the final value for the geometric parameter (bond distance, bond angle etc.) to the ideal value, taken from the dictionary.¹³

Table S3. Crystallographic statistics for data obtained from hen egg white lysozyme crystals grown on-chip and analyzed at room temperature.

	Hen egg white lysozyme (crystals grown and data collected on chip at room temperature)
Data collection	
Space group	P4 ₃ 2 ₁ 2
Cell dimensions	
a, b, c (Å)	78.876, 78.876, 37.957
α , β , γ (°)	90, 90, 90
Resolution (Å)	50 – 1.35 (1.40 – 1.37)
R_{merge}	0.080
Mean $I/\sigma I$	5.1 (2.33)
Completeness (%)	99.7 (99.9)
Redundancy	3.4 (3.3)
CC _{1/2}	0.991 (0.988)
CC*	0.998 (0.945)
Refinement	
Resolution (Å)	39.47- 1.35 (1.385 – 1.35)
Unique reflections	25547 (1852)
$R_{\text{work}} / R_{\text{free}}$ (%)	16.904/18.746
No. atoms	
Protein	1001
Water	59
Ligand	-
Ramachadran plot	
In preferred regions (%)	97.64
In allowed regions (%)	2.36
Outliers (%)	0.00
B -factors	
Protein	20.72
Water	30.43
Ligand	-
R.M.S. deviations	
Bond lengths (Å)	0.0151
Bond angles (°)	2.0276

^a Statistics for the high-resolution shell are indicated between brackets

^b Comparison of the final value for the geometric parameter (bond distance, bond angle etc.) to the ideal value, taken from the dictionary.¹³

References

- 1 E. D. Greaves and A. Manz, *Lab Chip*, 2005, **5**, 382–391.
- 2 J. H. Hubbell, *Phys. Med. Biol.*, 1999, **44**, R1.
- 3 J. H. Hubbell and S. M. Seltzer, *Tables of X-ray mass attenuation coefficients and mass energy-absorption coefficients 1 keV to 20 MeV for elements Z= 1 to 92 and 48 additional substances of dosimetric interest*, National Inst. of Standards and Technology-PL, Gaithersburg, MD (United ..., 1995.
- 4 C. W. Carruthers Jr, C. Gerdt, M. D. Johnson and P. Webb, *PLoS One*, 2013, **8**, e82298.
- 5 K. Dhouib, C. K. Malek, W. Pflöging, B. Gauthier-Manuel, R. Duffait, G. Thuillier, R. Ferrigno, L. Jacquamet, J. Ohana and J.-L. Ferrer, *Lab Chip*, 2009, **9**, 1412–1421.
- 6 J. M. García-Ruiz, F. Otálora, M. L. Novella, J. A. Gavira, C. Sauter and O. Vidal, *J. Cryst. Growth*, 2001, **232**, 149–155.
- 7 C. Hansen and S. R. Quake, *Curr. Opin. Struct. Biol.*, 2003, **13**, 538–544.
- 8 C. Sauter, F. Otálora, J. A. Gavira, O. Vidal, R. Giegé and J. M. García-Ruiz, *Acta Crystallogr. Sect. D Biol. Crystallogr.*, 2001, **57**, 1119–1126.
- 9 F. Pinker, M. Brun, P. Morin, A.-L. Deman, J.-F. Chateaux, V. Oliéric, C. Stirnimann, B. Lorber, N. Terrier and R. Ferrigno, *Cryst. Growth Des.*, 2013, **13**, 3333–3340.
- 10 M. J. Anderson, C. L. Hansen and S. R. Quake, *Proc. Natl. Acad. Sci.*, 2006, **103**, 16746–16751.
- 11 Q. Liu and W. A. Hendrickson, *Acta Crystallogr. Sect. D Biol. Crystallogr.*, 2013, **69**, 1314–1332.
- 12 Q. Liu, T. Dahmane, Z. Zhang, Z. Assur, J. Brasch, L. Shapiro, F. Mancina and W. A. Hendrickson, *Science (80-.)*, 2012, **336**, 1033–1037.
- 13 M. D. Winn, C. C. Ballard, K. D. Cowtan, E. J. Dodson, P. Emsley, P. R. Evans, R. M. Keegan, E. B. Krissinel, A. G. W. Leslie and A. McCoy, *Acta Crystallogr. Sect. D Biol. Crystallogr.*, 2011, **67**, 235–242.